pH-Independent Production of Hydroxyl Radical from Atomic H*-Mediated Electrocatalytic H2O2 Reduction: A Green Fenton Process without Byproducts

Zeng Huabin, Zhang Gong, Ji Qinghua, Liu Huijuan, Hua Xin, Xia Hua, Sillanpää Mika, Qu Jiuhui

DOI: 10.1021/acs.est.0c04694

pH-Independent Production of Hydroxyl Radical from Atomic H*-Mediated Electrocatalytic H_2O_2 Reduction: A Green Fenton Process without Byproducts

Huabin Zeng [a, b], Gong Zhang [a*], Qinghua Ji [a], Huijuan Liu [a], Xin Hua [c], Hailun Xia [c], Mika Sillanpää [d], Jiuhui Qu [a]

[a] Center for Water and Ecology, State Key Joint Laboratory of Environment Simulation and Pollution Control, School of Environment, Tsinghua University, Beijing 100084, China

[b] Department of Separation Science, School of Engineering Science, Lappeenranta-Lahti University of Technology LUT, Sammonkatu 12, FI-50130 Mikkeli, Finland

[c] Key Laboratory for Advanced Materials & School of Chemistry and Molecular Engineering, East China University of Science and Technology, Shanghai 200237, China

[d] Department of Civil and Environmental Engineering, Florida International University, Miami, USA

*Corresponding author:

Center for Water and Ecology, State Key Joint Laboratory of Environment Simulation and Pollution Control,

School of Environment, Tsinghua University,

Beijing 100084, China

E-mail address: gongzhang@mail.tsinghua.edu.cn

Table of Contents

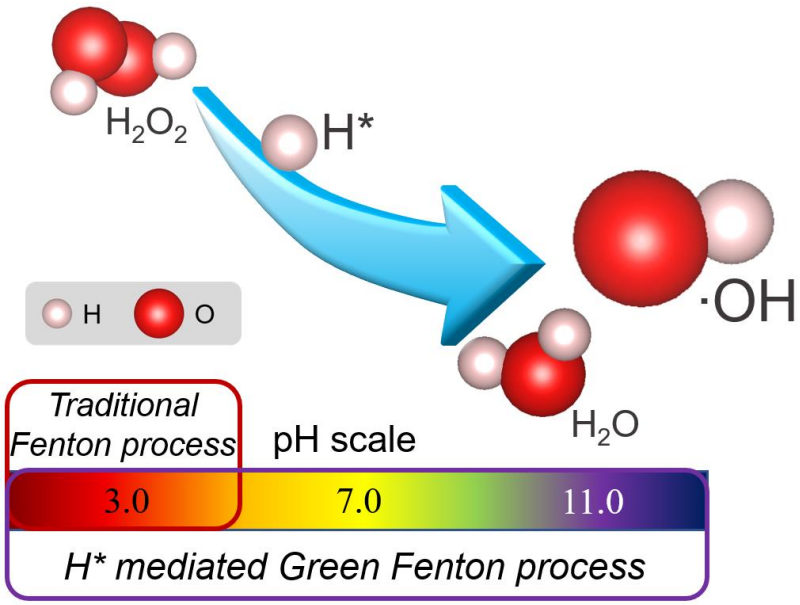

Abstract

Hydroxyl radical (·OH) can hydroxylate or dehydrogenate organics without forming extra products, thereby expediently applied in extensive domains. Although it can be efficiently produced through single-electron transfer from transition metal-containing activators to hydrogen peroxide (H_2O_2), narrow applicable pH range, strict activator/H_2O_2 ratio requirement, and byproducts that are formed in mixture with the background matrix, necessitate the need for additional energy-intensive up/downstream treatments. Here, we show a green Fenton process in an electrochemical cell, where the electro-generated atomic H* on a Pd/graphite cathode enables the efficient conversion of H_2O_2 into ·OH and subsequent degradation of organic pollutants (80% efficiency). Operando liquid time-of-fight secondary ion mass spectrometry verified that the H_2O_2 activation takes place through a transition state of the Pd-H*-H_2O_2 adduct with a low reaction energy barrier of 0.92 eV, whereby the lone electron in atomic H* can readily cleave the peroxide bridge, with ·OH and H_2O as products (ΔG_r=-1.344 eV). Using H^+ or H_2O as the resource, we demonstrate that the well-directed output of H* determines the pH-independent production of ·OH for stable conversion of organic contaminants in wider pH ranges (3~12). The research pioneers a novel path for eliminating the restrictions that are historically challenging in traditional Fenton process.

1. INTRODUCITON

Hydroxyl radical (·OH), as a non-selective radical, has played pivotal parts in the domains of water purification,[1] protein modification,[2] material preparation,[3] molecular synthesis,[4] and tumor therapy[5] throughout the past century (**Fig. 1**). Well known as Fenton process and Fenton-like processes, heterolytically cleaving the hydrogen peroxide (H_2O_2) by singlet-electron transfer from transition metal activators attracted much attention for their nature to yield ·OH under low operating cost and moderate working conditions, among which the most presentative system mainly proceeded via Fe(II)-initiated Fenton reaction or Fe(III)-catalytic Haber–Weiss reaction.[6] Highly efficient Fenton process have been accordingly restricted by the narrow applicable pH range and need for a suitable Fe^{2+}/H_2O_2 ratio,[7] whereby the electron in Fe(II) ions can be made available for specific cleavage of the peroxide bridge in H_2O_2 rather than the unsatisfactory quenching of as-produced ·OH. Moreover, this reaction and its derivative (Fenton-like reaction) inevitably results in the production of byproducts in mixture with the background matrix, such as iron sludge production for environmental remediation,[1] increased purification difficulty of target products for protein modification and chemosynthesis,[2-4] and toxicity of byproducts (Cu^{2+}) to healthy tissue for tumor therapy.[5] The phenomena are inherently regarded as another knotty problem.

In its use in water purification, neutralization of as-treated water and disposal of byproducts (iron sludge) certainly will impose further financial burden.[7] At the meantime, it is difficult to meet the optimized conditions for efficient Fenton reactions, especially in the human body or a chemosynthesis reactor. In addition to the removal of as-produced byproducts, the difference in atmosphere is also a complication for the effective output of ·OH in the domains of tumor therapy or chemosynthesis.[8] Although these problems seemed to be alleviated by substitution of the

homogeneous Fenton reaction with the heterogeneous Fenton reaction,[5, 9] the rapid inactivation and serious metal leaching of heterogeneous activators leads to short-lived Fenton processes. To complement advancements in these fields, breakthroughs in achieving a byproduct-free, stable and efficient H_2O_2 activation process that can operate at wide pH range are therefore urgently desired. In view that the Fenton process preferably takes place in aqueous solution, the byproduct-free activators must be only comprised of hydrogen (H), oxygen (O) or the derivatives.[10] Unfortunately, as a two-electron acceptor, H_2O_2 is more readily converted to the useless H_2O molecule via the two-electron reduction path,[11] whereas the useful product (·OH) with high oxidation ability will be harvested only if reaction proceeds through the one-electron reduction path. We thus focus on well-known atomic H*, a one-electron donor, which possesses a redox potential (−2.10 V *vs* RHE) that enables rapid transfer of an electron to H_2O_2,[12, 13] with ·OH and H_2O as products. Theoretical calculations unravel that the reaction energy for this H_2O_2 activation is -1.344 eV, indicating that the reaction can proceed spontaneously.

Atomic H^*, a critical intermediate during the electrocatalytic water splitting reaction, can be regularly produced through tuning the applied voltage.[14] However, as highlighted by the typical volcano plot for the hydrogen evolution reaction (HER), the as-generated atomic H* (Volmer reaction) species prefer to bond with each other for subsequent H_2 evolution (Heyrovsky reaction). We therefore applied a strategy in which we would seek to optimize the formation energy required for active metal sites to reach the desired H_2 evolution, so that the generation of adsorbed (*ads*) or absorbed (*abs*) H* in vicinity to the cathode can be utilized as a well-directed activator for efficient conversion of H_2O_2 into ·OH, and the as-produced ·OH in this well-controlled activation approach refrains from fast quenching in the conventional transition metal ion-initiated Fenton or Fenton-like reactions.[15] More importantly, the formation of atomic H^* is independent of solution pH. In

acidic conditions, atomic H* comes from the reduction of H^+, while H_2O is the precursor in neutral or alkaline solution, so that the H_2O_2 decomposition process can be extended to all pH levels. Consistent with the theoretically predicted path $H^* + H_2O_2 \rightarrow \cdot OH + H_2O$, operando liquid time-of-fight secondary ion mass spectrometry (ToF-SIMS) further verifies that the reaction takes place via the transition state of the Pd-H*-H_2O_2 adduct when using palladium (Pd) as mediator, thereby lone electron in atomic H* is ready to inject into H_2O_2 to cleave the peroxide bridge. Using a scaled atomic H*-rich cathode, we demonstrate production of ·OH for stable oxidation of aqueous organic contaminants which can be easily tuned by changing applied potential. In view that atomic H* can be well-confined on the cathode over the entire pH range, the continuous supplement of a certain amount of atomic H* from this electro-reduction configuration is an ideal approach for efficient activation of H_2O_2 through a one-electron reduction path.

2. EXPERIMENTAL SECTION

Materials preparation. The Pd/graphite electrode was prepared by magnetron sputtering of a Pd thin film with a thickness of 200 nm, followed by calcining at 200 ˚C for 120 min under hydrogen atmosphere to firmly adhere the Pd film to the graphite substrate.

For electrochemical analysis, Pd/C particles were obtained by a chemical deposition approach. 1 mmol K_2PdCl_6 and 8 mmol sodium citrate were first dissolved in 200 mL ultrapure water. Then, ~400 mg of activated carbon (AC) was dispersed in the solution with ultrasonication for 30 min. Next, 100 ml $NaBH_4$ with concentration of 100 $mmol \cdot L^{-1}$ was added dropwise to the above solution. The obtained Pd/AC catalyst was filtered and washed, and finally dried in a vacuum oven at 60 °C overnight.

Electrochemical analysis. In order to obtain a homogenous ink, 5 mg of the Pd/C catalyst was dispersed in 1 mL of a Nafion-containing solution (comprised of 750 μL of water, 200 μL of

isopropanol, and 50 μL of 5% Nafion solution) under ultrasonication for 30 min. A working electrode was then prepared by dripping 5 μL of the catalytic ink on a glassy carbon electrode (3 mm in diameter) and drying at ambient temperature. Before electrochemical analysis, the working electrode was activated by continuous CV cycling between -0.20 and 0.9 V at a scan rate of 100 mV s^{-1} in a N_2-saturated 0.1 M $HClO_4$ solution until a stable voltammogram was obtained.

Characterization. ESR analysis was carried out using a Bruker EPR 300E spectrometer with a microwave bridge (receiver gain, 1×105; modulation amplitude, 2 G; microwave power, 10 mW; modulation frequency, 100 kHz). The concentration of organics was determined by high performance liquid chromatography (HPLC). The mobile phase and wavelength for organics detection are displayed in **Table S3.** The Pd leaching was quantified by ICP-OES analysis. The degradation intermediates during the chemical conversion process were identified by LC-MS analysis. Total organic carbon (TOC) was measured using a Shimadzu TOC analyzer (TOC-VCPH, Shimadzu, Japan).

Operando ToF SIMS analysis. The vacuum compatible micro-electrochemical cell was prepared using the strategy in work of Long et. al. with some necessary modifications.[16, 17] In brief, a liquid chamber with a size of 6.0 × 5.5 × 1.0 mm (length × width × depth) was fabricated using a Polydimethylsiloxane (PDMS) block. The quasi-reference electrode (QRE) and counter electrode (CE) were both made of Pt wires (0.5 mm diameter and ~ 4.0 mm effective length each). Pd working electrode (WE) was prepared with a 50 nm Pd layer on a 100 nm thick SiN membrane attached on a silicon frame (7.5 × 7.5 mm^2, thickness 200 μm) using a sputter coater. The area of WE is ~ 4 mm^2, which was connected to copper wires by conductive silver epoxy. The Pd-coated SiN membrane and PDMS micro-chamber were irreversibly bonded via air plasma. After a desired electrolyte was injected into the micro-electrochemical cell slowly with a micro-injector, cell was

sealed and then transferred into main-chamber of ToF-SIMS for *in-situ* characterization. Operando ToF-SIMS analysis was conducted on a ToF-SIMS V spectrometer (IONTOF GmbH, Germany). A 30 keV Bi_3^+ primary ion beam with a target current of 0.35 pA was used for all analysis. Analysis area was a circle with a diameter of 2 μm. Positive mass spectra were calibrated using CH^+, CH_2^+, CH_3^+, $C_2H_3^+$ and $C_2H_5^+$.

Theoretical calculations. All the calculations were performed within the framework of density functional theory as implemented in the Vienna Ab initio Software Package (VASP 5.3.5) code with the Perdew-Burke-Ernzerhof generalized gradient approximation and the projected augmented wave (PAW) method. The Brillouin zone of the surface unit cell was sampled by Monkhorst-Pack grids, with a different k-point mesh for Pd bulk and Pd(111) structure optimizations. Bulk-structured Pd and a Pd(111) facet were determined by 15×15×15 and 3×3×1 Monkhorst-Pack grids. Our calculated equilibrium lattice constant for bulk Pd is 3.920 Å. The convergence criterion for electronic self-consistent iteration and force was set to 10^{-5} eV and 0.01 eV/Å. The climbing image nudged elastic band method was used to confirm the transition states, with one imaginary frequency along with reaction coordinates. A 4×4 supercell of the Pd(111) surface including 4 atomic layers was constructed to model the Pd catalyst in this work, with the bottom two layers fixed in structural relaxation. A vacuum layer of 12 Å was introduced to avoid interactions between periodic images.

The adsorption energy (E_{ads}) of the surface species is defined by:

$$E_{ads} = E_{total} - E_{surface} - E_{species},$$

where E_{total} represents the total energy of the adsorbed species with catalyst surface, $E_{surface}$ is the energy of the empty Pd(111) surface, and $E_{species}$ is the energy of the species in the gas phase.

3. RESULTS AND DISCUSSION

Activation Feasibility of H_2O_2 with atomic H*. To experimentally verify this electrochemical conversion process, Pd/C catalyst from a modified chemical deposition method was applied for *in situ* electrochemical monitoring the fate of atomic H* (**Text. S1**). SEM and XPS analysis of the Pd/C catalyst revealed that Pd nanoparticles were tightly attached to the conductive carbon particles (**Fig. S1**). Meanwhile, exposure of Pd (111) facets theoretically endowed the catalyst with a high capacity for the provision of atomic H* with the application of a negative potential.[18] Before cyclic voltammetry (CV) analysis, working electrode with a thin film of Pd/ C catalyst on a rotating disk glassy carbon electrode was activated through continuous CV cycles until a stable voltammogram was obtained (**Text. S2**, **Fig. S2**). With varying starting potentials from -0.70 V to -1.20 V (vs Ag/AgCl, the same below) during CV analysis, the generated H* species in the reduction stage were oxidized in oxidation stage. **Fig. 2a** shows three oxidation peaks in positive scans, located in potential ranges of −0.80 to −0.60 V, −0.30 to −0.10 V, and −0.10 to 0.10 V. These peaks referred to the oxidation of molecular H_2 at −0.80 V, absorbed H^*_{abs} at −0.30 V, and adsorbed H^*_{ads} at −0.10 V (**Fig. S3**), respectively.[19] With the addition of H_2O_2, the observed oxidation peak for H^*_{abs} at -0.30 V was derived from the generation of atomic H* via *Volmer* process, while the disappeared peak for H^*_{ads} at -0.10 V was mainly due to fact that H_2O_2 strongly scavenged H^*_{ads} (**Fig. 2b**).

A two-cell electrochemical reactor was constructed for direct identification of the produced radical in the reaction of H_2O_2 with atomic H* using Pd/graphite as working electrode (cathode), Ag/AgCl electrode as reference electrode and graphite as the counter electrode (**Text. S3**). Electron spin resonance (ESR) analysis using 5,5-dimethyl-1-pyrroline N-oxide (DMPO) as spin-trapping reagent has been performed in various systems.[20] As shown in **Fig. 2c**, nine characteristic peaks of

DMPO-H were observed in the electro-reductive system using Pd/graphite cathode,[17] indicating the formation of atomic H*. After the introduction of H_2O_2 into the system, a typical four-line ESR spectrum of DMPO-OH with an intensity of 1:2:2:1 was recorded while the signals of DMPO-H disappeared,[21] suggesting the emergence of ·OH with consumption of atomic H*. At the meantime, the conversion pathway of a typical molecule, 2,4-dichlorphenol (2,4-DCP), were analyzed using liquid chromatography-mass spectrometry (LC-MS) to identify the reactive species in this system (**Text. S4**). In the absence of H_2O_2, only the intermediate of phenol can be detected in the degradation process (**Fig. S5**), which was representative product of atomic H* dominated dechlorination reaction.[19] In the presence of H_2O_2, the products of 3,5-dichloro-1,2-hydroquinone, 4,6-dichloro-1,3-hydroquinone, or 2,4-dichloro-1,3-hydroquinone were resulted from the electrophilic hydroxylation of 2,4-DCP at ortho- and para- positions, which was identical to the ·OH oxidation mechanism (**Table. S1**).[22] The result further confirmed that a considerable amount of H_2O_2 was activated to ·OH with the sacrifice of atomic H*.

Operando ToF-SIMS analysis. For better understanding of activation mechanism of H_2O_2 on Pd cathode at a molecular level, we used a micro-electrochemistry (micro-EC) cell (**Fig. S6**) to couple with the operando liquid time-of-flight secondary ion mass spectrometry (ToF-SIMS).[23] In this micro-EC cell, a 50 nm-thick Pd layer was used as working electrode (WE), and Pt filaments were respectively applied as counter electrode (CE) and quasi-reference electrode (QRE). After being filled with deoxygenated H_2O_2 solution at a solution pH of 3.0, the whole cell was sealed and mounted onto a customized sample holder before placing in the ToF-SIMS vacuum chamber. A 2 μm micropore for sampling was drilled through the Pd-coated SiN membrane using a focused Bi_3^+ primary ion beam (**Fig. 3a)**. Surface tension would hold the liquid in the micropore, preventing fast evaporation or splashing of liquid.[16] Thus, the micropore allows *in-situ* analysis of the

electrode-electrolyte interface (EEI) during a dynamic potential scan by ToF-SIMS analysis. The micro-EC cell was connected to an electrochemical workstation outside of vacuum, allowing the application of a potential on the Pd-coated micro electrode.

Under the open-circuit potential, some regular secondary ions, including solvated proton species ($H^+(H_2O)_n$), could be detected, and their intensities were relatively constant as the time progressed, indicating the formation of stable EEI due to self-renewable liquid surface (**Fig. S7**). After the stabilization of the *in-situ* monitor system on EEI, consecutive CV scans between 0.2 V to -0.8 V were performed on the working electrode for operando discrimination of the critical intermediates on the Pd cathode under given potential conditions. With CV scans applied, Pd-containing species that appeared, such as Pd^+, $(Pd\text{-}H_2)^+$ and $(Pd\text{-}H)^+$, were mainly derived from adsorbed ions or molecules on the Pd surface. In order to correct the slight shift from the effect of charge accumulation or microbubbles produced during the signal collection process, the observed peaks were subsequently normalized via comparison of their intensities with the intensity of the Pd^+ reference. As shown in **Fig. S8**, the intensity of the peak for $(Pd\text{-}H_2)^+$, referring to hydrogen evolution reaction, showed a periodic change with the variation of applied potential. At negative potential, the intensity achieved at the peak value increased at the potential of -0.8 V, while it regressed to original level near 0.2 V. As secondary precursor of $Pd\text{-}H_2$, the intensity of Pd -H* should theoretically exhibit a similar trend as $Pd\text{-}H_2$. Differently, the normalized intensity of Pd-H* was almost maintained at the same level in the following scans. Moreover, in view fact that Pd is associated with a superior catalytic Volmer reaction (H*), the peak fluctuation ought to be more dramatic in contrast to that for $Pd\text{-}H_2$. However, the difference between the peak (at negative potential) and valley (at positive potential) seemed to be weakened. These abnormal phenomena might be reasonably ascribed to as-generated H* being *in-situ* converted by the H_2O_2.

At the meantime, a signal assigned to Pd-H_3O_2 appeared at the open-circuit potential. Remarkably, with the negative potentials applied on the working Pd electrode, the intensity was increased and accordingly reached a peak at the potential of -0.8 V (**Fig. 3b**). Similarly, we also recorded the signal change of Pd-H_3O_2 with varying applied potential, and the intensity was periodically changed when the potential cycled back to 0.2 V. However, in sharp contrast to the gentle variation in Pd-H intensity, the violently fluctuating peak suggested that the Pd-H_3O_2 was a combination of atomic H* on Pd surface and H_2O_2 from solution, which should be the critical intermediate in the pathway of H* + H_2O_2 → ·OH + H_2O. Furthermore, density functional theory (DFT) calculations were simultaneously performed to elucidate H_2O_2 activation process. Due to the favorable bonding of H* in the Pd (111) lattice, only the energy barrier of ~0.92 eV was required for formation of the Pd-H_3O_2 adduct (**Fig. 3e**). In a subsequent step, rapid electron transfer between atomic H* and H_2O_2 spontaneously took place, according to the charge density analysis (**Fig. 3d**), with a negative reaction energy of -1.67 eV. The O-O bond ($l_{O\text{-}O}$) of Pd-H*-H_2O_2 adduct is lengthened from 1.469 Å (H_2O_2) to 1.730 Å, indicating the cleavage of the O-O bond in the H_2O_2-H* adduct accompanied with the formation of ·OH and H_2O. With further consecutive CV scans, the intensity of Pd-H_3O_2 exhibited period changes, indicating that the generation of Pd-H_3O_2 can be easily tuned simply by changing the applied potential.

Application of green process for organics degradation. Based on the mechanism revealed above for green Fenton, we utilized a two-cell electrochemical reactor for producing ·OH and oxidizing organics under a deoxygenated atmosphere (**Fig. S9**).[24] Here, we used the refractory benzoic acid (BA) as the probe of ·OH due to its high kinetic rate constant for reaction with ·OH,[25] as well as its inertness to Pd-activated H_2O_2. As shown in **Fig. S10**, with the addition of 50 mmol·L^{-1} H_2O_2, 49.03% of BA was degraded using the Pd cathode at only -0.6 V (vs Ag /AgCl). A modified first-

249 order kinetics model (*k* value) based on the degradation rate was used to evaluate the activation of
250 H_2O_2. The higher *k* value (0.1567 h^{-1}) in the green Fenton process than the sum of those in the
251 individual processes (0.0291 $h^{-1}$and 0.0599 h^{-1}) indicates that the Pd-cathode and H_2O_2 had
252 synergetic effects on ·OH production (**Fig. 4a**). With an increase in the applied potential on cathode
253 to -1.2 V (vs RHE), the *k* value was further increased to 0.3327 h^{-1} owing to the increasing amount
254 of atomic H* on the Pd cathode with decreasing potential (**Fig. S11**). Meanwhile, TOC removal
255 increased from 0.029 ppm (-0.6 V) to 1.273 ppm (-1.2 V). Quenching experiments using methanol,
256 ethanol and O_2 revealed that ·OH and atomic H* played significant roles in the oxidation process
257 of BA by H_2O_2 (**Fig. S12**).[26-28] In particular, the nearly complete inhibition of BA degradation by
258 methanol and ethanol excluded the possibility of a non-radical oxidation process or other reactive
259 oxygen radicals. The results are consistent with the role of ·OH as reactive oxygen radical and
260 atomic H* as an activator for H_2O_2 in the green Fenton process. The system was further evaluated
261 by degrading several model pollutants. As shown in **Fig. S13**, all the organics could be almost
262 completely degraded in 3 h at a low potential. Moreover, the green Fenton process with negligible
263 loss of catalytic sites (Pd concentration in solution was lower than detection limit of inductively
264 coupled plasma atomic emission spectroscopy) can be applied in various working conditions.
265 Pd/graphite electrode was revealed to be stable enough by comparing the Pd species and most
266 exposed facet of the used electrode with fresh one (**Text S5**), the Pd species and Pd facet were
267 shown to be Pd^0 and Pd(111) through the green Fenton reaction.
268 More importantly, a strict pH requirement in conventional Fenton or Fenton-like ·OH production
269 processes is mainly due the fact that the active species (*eg.* $FeOH^+$ in Fenton process or $\equiv FeOH_2^+$
270 in FeOOH-Fenton process) is readily deactivated when the operation condition deviated from
271 optimized pH,[29, 30] which results in extra financial input for adjusting pH value (**Table S2**).

However, the atomic H* comes from the reduction of H^+ ions in acidic conditions, while H_2O is the precursor in neutral or alkaline solution. According to results of CV scans under different pH conditions, the peaks attributed to H^*_{ads} and H^*_{abs} can be easily observed at characteristic potentials (**Fig. 4b**). After addition of H_2O_2, the sharp decrease in H^*_{ads} intensity indicates that the activation of H_2O_2 by atomic H* can take place over a wide pH range. For comparing the sensitivity of different ·OH production systems to pH, we standardized the kinetic constants by dividing these values by optimal kinetic constant and plotted the relative *k* vs solution pH in various processes. In stark contrast to the narrow pH application range for the conventional Fenton or Fenton-like reaction, **Fig. 4c** shows that green Fenton has gentlest change on the relative *k* in a wider pH range due to the inherent nature of atomic H*. The property can lower the cost of water purification or other applications on the pH adjustment to optimal pH before the reaction, and to circumneutral condition after the reaction, compared to traditional Fenton process.

ASSOCIATED CONTENT

Supporting information

Supporting information is available for this paper, including 5 Texts, 15 Figures, and 4 Tables.

Author information

Corresponding authors

Gong Zhang: gongzhang@mail.tsinghua.edu.cn

Notes

The authors declare no competing interests.

Acknowledgements

The authors acknowledge financial support by National Natural Science Foundation of China (No. 22022606, 51722811, 51738013, 51978371), National Water Pollution Control and Treatment Science and Technology Major Project 2018ZX07110007 and Guangxi Bagui Scholar' Construction Project (Grant/Award Number: 2016A10).

References

(1) Yang, X.; Xu, X.; Xu, J.; Han, Y. Iron Oxychloride (FeOCl): An Efficient Fenton-Like Catalyst for Producing Hydroxyl Radicals in Degradation of Organic Contaminants. *J. Am. Chem. Soc.* **2013**, 135, 16058-16061.

(2) Xu, G. H.; Chance, M. R. Hydroxyl Radical-Mediated Modification of Proteins as Probes for Structural Proteomics. *Chem. Rev.* **2007**, 107, 3514-3543.

(3) Feng, G.; Cheng, P.; Yan, W. F.; Boronat, M.; Li, X.; Su, J. H.; Wang, J. Y.; Li, Y. Corma, A.; Xu, R. R.; Yu, J. H. Accelerated Crystallization of Zeolites via Hydroxyl Free Radicals. *Science* **2016**, 351, 1188-1191.

(4) Chen, M. S.; White, M. C. A Predictably Selective Aliphatic C-H Oxidation Reaction for Complex Molecule Synthesis. *Science* **2007**, 318, 783-787.

(5) Tang, Z.; Liu, Y.; He, M.; Bu, W. Chemodynamic Therapy: Tumour Microenvironment-Mediated Fenton and Fenton-Like Reactions. *Angew. Chem. Int. Edit.* **2019**, 58, 946-956.

(6) Haber, F.; Weiss, J. Über Die Katalyse Des Hydroperoxydes. *Naturwissenschaften.* **1932**, 20, 948-950.

(7) Chen, L. W.; Ma, J.; Li, X. C.; Zhang, J.; Fang, J. Y.; Guan, Y. H.; Xie, P. C. Strong Enhancement on Fenton Oxidation by Addition of Hydroxylamine to Accelerate the Ferric and Ferrous Iron Cycles. *Environ. Sci. Technol.* **2011**, 45, 3925-3930.

(8) Lin, L. S.; Huang, T.; Song, J. B.; Ou, X. Y.; Wang, Z. T.; Deng, H. Z.; Tian, R.; Liu, Y. J.; Wang, J. F.; Liu, Y.; Yu, G. C.; Zhou, Z. J.; Wang, S.; Niu, G.; Yang, H. H.; Chen, X. Y. Synthesis of

Copper Peroxide Nanodots for H_2O_2 Self-Supplying Chemodynamic Therapy. *J. Am. Chem. Soc.* **2019**, 141, 9937-9945.

(9) Pouran, S. R.; Raman, A. A. A.; Daud, W. Review on the Application of Modified Iron Oxides as Heterogeneous Catalysts in Fenton Reactions. *J. Clean. Prod.* **2014**, 64, 24-35.

(10) Noyori, R. Pursuing Practical Elegance in Chemical Synthesis. *Chem. Communications*. **2005**, 1807-1811.

(11) Chen, S.; Yuan, R.; Chai, Y.; Hu, F. Electrochemical Sensing of Hydrogen Peroxide Using Metal Nanoparticles: A Review. *Microchim. Acta.* **2013**, 180, 15-32.

(12) Lee, J. Y.; Lee, J. G.; Lee, S. H.; Seo, M.; Piao, L.; Bae, J. H.; Lim, S. Y.; Park, Y. J.; Chung, T. D. Hydrogen-Atom-Mediated Electrochemistry. *Nat. Commun.* **2013**, 4, 2766.

(13) Pan, Y.; Su, H. R.; Zhu, Y. T.; Molamahmood, F. V.; Long, M. CaO_2 Based Fenton-Like Reaction at Neutral pH: Accelerated Reduction of Ferric Species and Production of Superoxide Radicals. *Water Res.* **2018**, 145, 731-740.

(14) Zheng, Y.; Jiao, Y.; Jaroniec, M.; Qiao, S. Z. Advancing the Electrochemistry of the Hydrogen-Evolution Reaction through Combining Experiment and Theory. *Angew. Chem. Int. Edit.* **2015**, 54, 52-65.

(15) Li, W. J.; Ma, H. Y.; Huang, L. H.; Ding, Y. Well-Defined Nanoporous Palladium for Electrochemical Reductive Dechlorination. *Phys. Chem. Chem. Phys.* **2011**, 13, 5565-5568.

(16) Wang, J. G.; Zhang, Y. Y.; Yu, X. F.; Hua, X.; Wang, F. Y.; Long, Y. T.; Zhu, Z. H. Direct Molecular Evidence of Proton Transfer and Mass Dynamics at the Electrode-Electrolyte Interface. *J. Phys. Chem. Lett.* **2019**, 10, 251-258.

(17) Hua, X.; Xia, H. L.; Long, Y. T. Revisiting a Classical Redox Process on a Gold Electrode by Operando ToF-SIMS: Where Does the Gold Go? *Chem. Sci.* **2019**, 10, 6215-6219.

(18) Quaino, P.; Santos, E. Hydrogen Evolution Reaction on Palladium Multilayers Deposited on Au(111): A Theoretical Approach. *Langmuir* **2015**, 31, 858-867.

(19) Liu, R.; Zhao, H. C.; Zhao, X. Y.; He, Z. L.; Lai, Y. J.; Shan, W. Y.; Bekana, D.; Li, G.; Liu, J. F. Defect Sites in Ultrathin Pd Nanowires Facilitate the Highly Efficient Electrochemical Hydrodechlorination of Pollutants by H^*_{ads}. *Environ. Sci. Technol.* **2018**, 52, 9992-10002.

(20) Chen, Y.; Zhang, G.; Liu, H. J.; Qu, J. H. Confining Free Radicals in Close Vicinity to Contaminants Enables Ultrafast Fenton-Like Processes in the Interspacing of MoS_2 Membranes. *Angew. Chem. Int. Edit.* **2019**, 58, 8134-8138.

(21) Yang, Z. C.; Qian, J. S.; Yu, A. Q.; Pan, B. C. Singlet Oxygen Mediated Iron-Based Fenton-Like Catalysis under Nanoconfinement. *Proc. Natl. Acad. Sci. USA.* **2019**, 116, 6659-6664.

(22) Chu, W.; Kwan, C. Y.; Chan, K. H.; Kam, S. K. A Study of Kinetic Modelling and Reaction Pathway of 2,4-Dichlorophenol Transformation by Photo-Fenton-Like Oxidation. *J. Hazard. Mater.* **2005**, 121, 119-126.

(23) Wang, J. G.; Hua, X.; Xia, H. L.; Long, Y. T. Pore Confined Liquid-Vacuum Interface for Charge Transfer Study in an Electrochemical Process. *Anal. Chem.* **2019**, 91, 3195-3198.

(24) Campos-Martin, J. M.; Blanco-Brieva, G.; Fierro, J. L. G. Hydrogen Peroxide Synthesis: An Outlook Beyond the Anthraquinone Process. *Angew. Chem. Int. Edit.* **2006**, 45, 6962-6984.

(25) Buxton, G. V.; Greenstock, C. L.; Helman, W. P.; Ross, A. B. Critical-Review of Rate Constants for Reactions of Hydrated Electrons, Hydrogen-Atoms and Hydroxyl Radicals ($\cdot OH/\cdot O^-$) in Aqueous-Solution. *J. Phys. Chem. Ref. Data.* **1988**, 17, 513-886.

(26) Guo, Z.; Xie, Y. B.; Xiao, J. D.; Wang, Y. X.; Xu, Z. M.; Zhang, Y.; Yin, L. C.; Cao, H. B.; Gong, J. L. Single-Atom Mn-N_4 Site-Catalyzed Peroxone Reaction for the Efficient Production of Hydroxyl Radicals in an Acidic Solution. *J. Am. Chem. Soc.* **2019**, 141, 12005-12010.

(27) Zhou, Y. J.; Zhang, G.; Ji, Q. H.; Zhang, W.; Zhang, J. Y.; Liu, H, J.; Qu, J. H. Enhanced Stabilization and Effective Utilization of Atomic Hydrogen on Pd-In Nanoparticles in a Flow-Through Electrode. *Environ. Sci. Technol.* **2019**, 53, 11383-11390.

(28) Hess, W. P.; Tully, F. P. Hydrogen-Atom Abstraction from Methanol by Hydroxyl Radical. *J. Phys. Chem.* **1989**, 93, 1944-1947.

(29) Voelker, B. M.; Sulzberger, B. Effects of Fulvic Acid on Fe(II) Oxidation by Hydrogen Peroxide. *Environ. Sci. Technol.* **1996**, 30, 1106-1114.

(30) Chou, S. S.; Huang, C. P.; Huang, Y. H. Heterogeneous and Homogeneous Catalytic Oxidation by Supported γ-FeOOH in a Fluidized Bed Reactor: Kinetic Approach. *Environ. Sci. Technol.* **2001**, 35, 1247-1251.

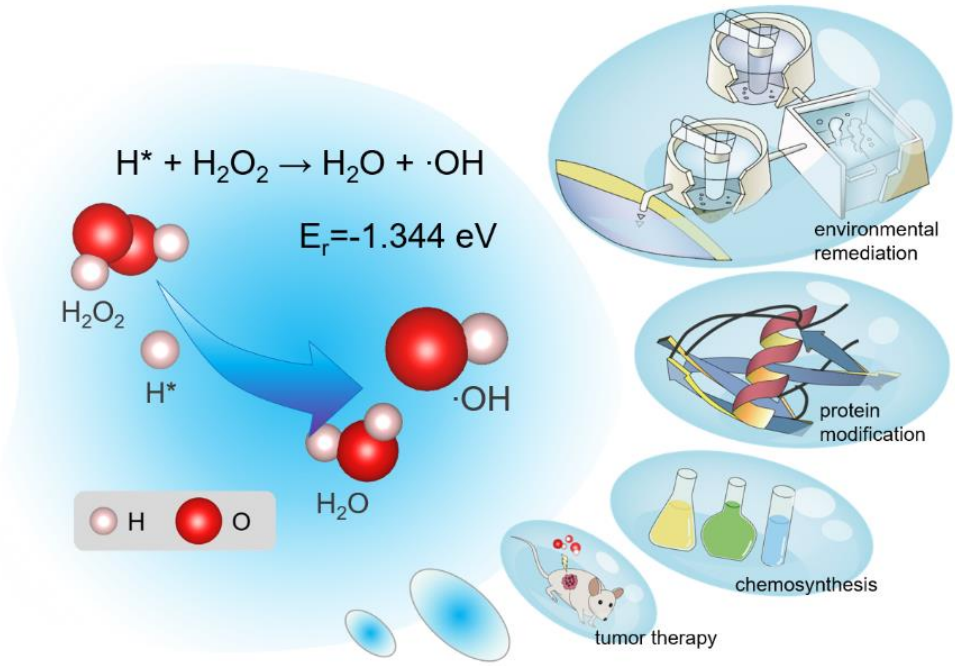

Fig. 1. Proposed mechanism for interaction between atomic H* and H_2O_2; the byproduct-induced negative effects caused by traditional metal activators for Fenton processes in various application scenarios. (iron sludge production for environmental remediation; increased purification difficulty of target products for protein modification and chemosynthesis; toxicity of byproducts to healthy tissue for tumor therapy)

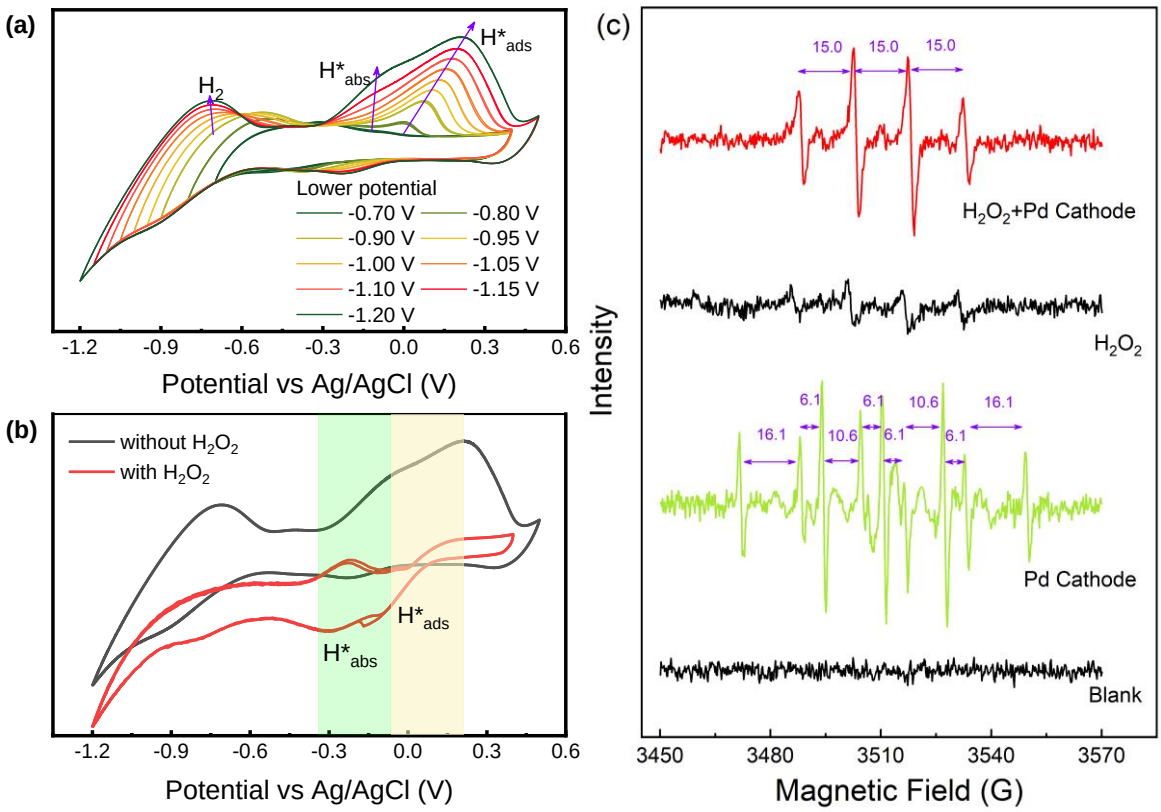

384

385

386 **Fig. 2**. The interaction of H_2O_2 with atomic H*. (a) Identification of various active hydrogen
387 species by CVs of Pd/C catalyst; (b) CVs of Pd/C catalyst without or with H_2O_2 addition; (H_2O_2,
388 4 mM; Na_2SO_4, 50 mmol·L^{-1}; solution pH, 7.0; scanning rate, 10 mV/s; deoxygenated atmosphere)
389 (c) reactive intermediates detection by ESR analysis in various systems. (Na_2SO_4, 50 mmol·L^{-1};
390 deoxygenated atmosphere)

391

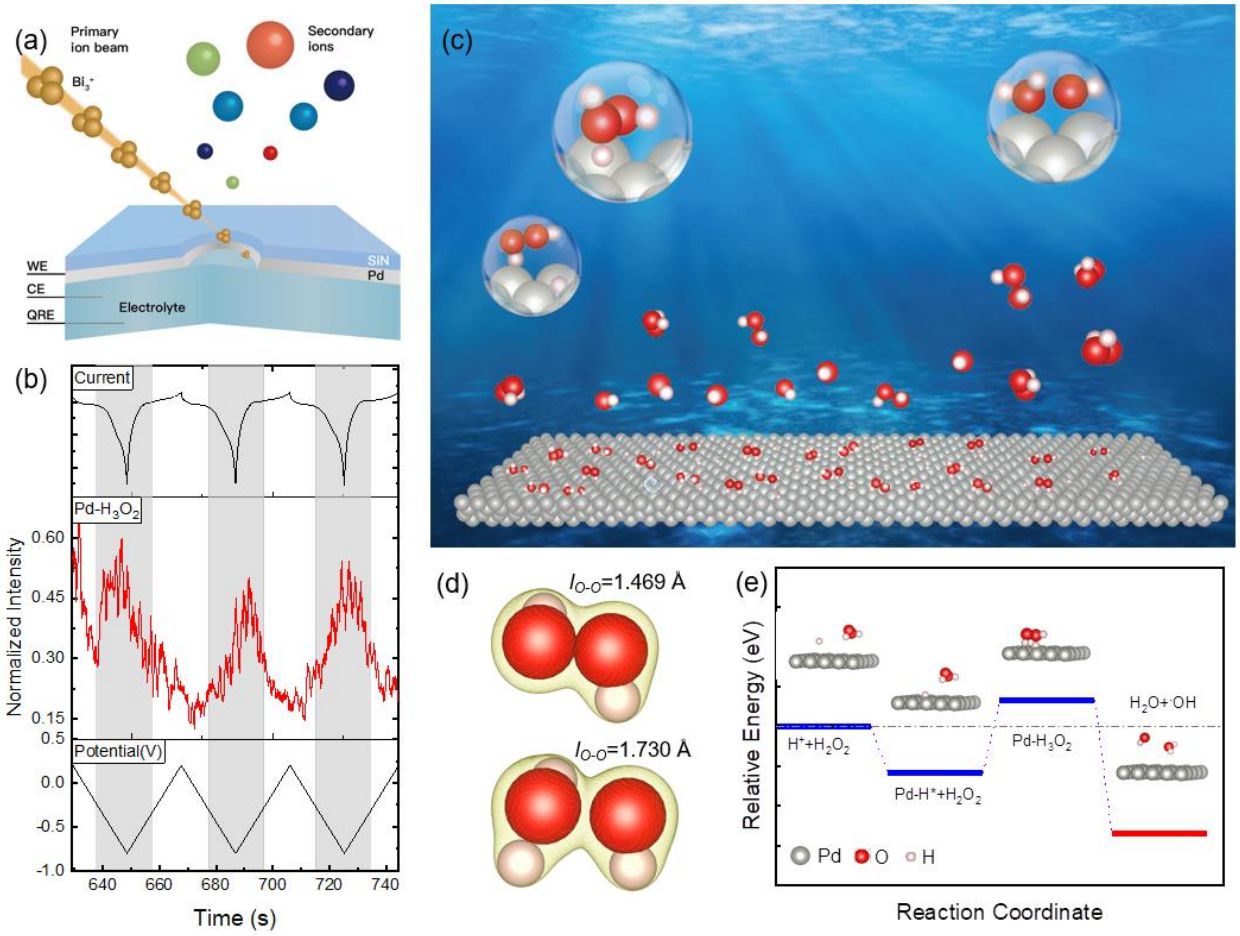

Fig. 3. Insight into the reaction mechanism of H_2O_2 with atomic H* on Pd surface. (a) Schematic of in-situ liquid ToF-SIMS coupled with an electrochemical workstation for monitoring EEI during Fenton process. (b) Intensity of Pd-H_3O_2 analyzed by ToF-SIMS during cyclic voltammetry in potential range from 0.20 to -0. 8 V. (3 cycles for CV; Na_2SO_4, 1 mmol·L^{-1}; H_2O_2, 5 mmol·L^{-1}; solution pH, 3.0) (c) Model of green Fenton process on the Pd(111) surface and the mechanism of the green Fenton process revealed by operando ToF-SIMS analysis; (d) Charge density difference of H_2O_2 and H*-H_2O_2 adduct. (e) Free energy change of the H*-initiated Fenton process on surface of Pd (111).

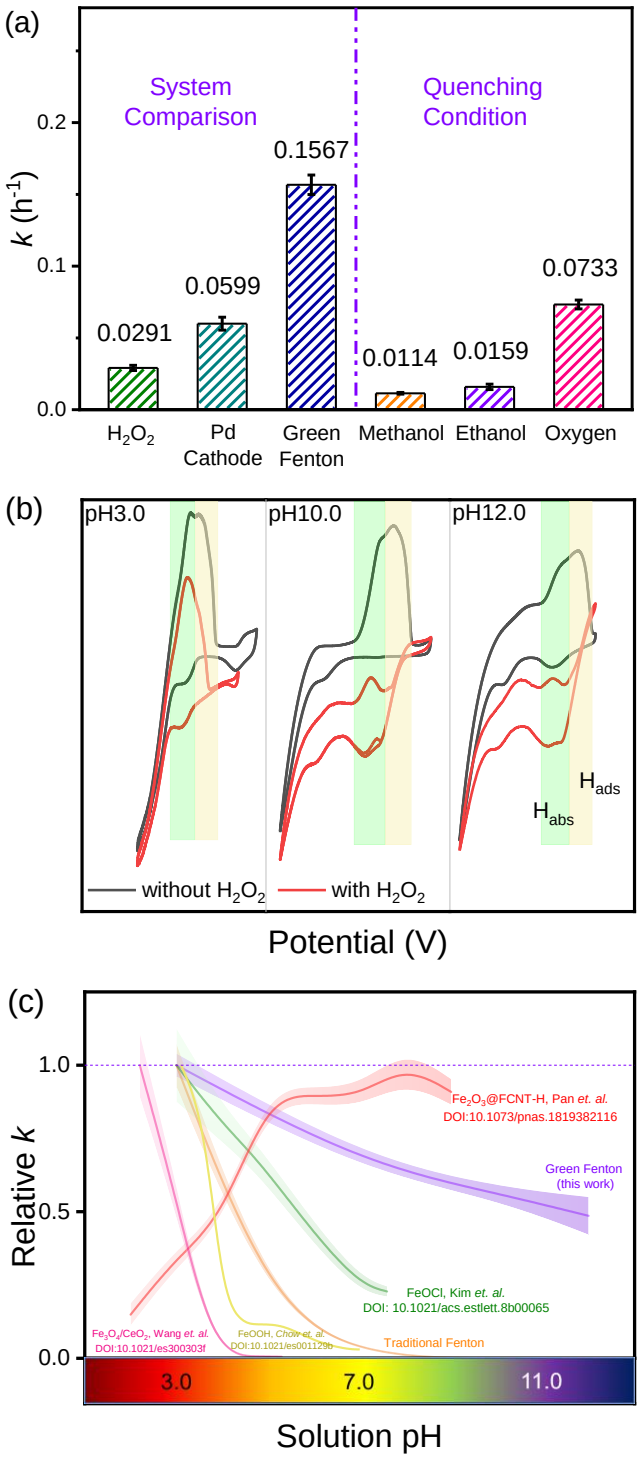

Fig. 4. Employment of green Fenton mechanism for organics degradation. (a) Comparison of k-values for BA degradation in various systems. (H_2O_2, mmol·L^{-1}; solution pH, 3.0; BA, 50 μmol·L^{-1}; applied potential, -0.6 V vs Ag/AgCl; Quenching agent, 1.0 mol·L^{-1}) (b) CVs of Pd/C catalyst with and without addition of H_2O_2. (H_2O_2, 4 mM; Na_2SO_4, 50 mmol·L^{-1}; scanning rate, 10 mV/s;

deoxygenated atmosphere) (c) Sensitivity comparison of green Fenton process with previous Fenton/Fenton-like processes to solution pH. (Relative *k* equals to the division of kinetic constants by that of optimal solution pH.)